Soft Matter

Analysis of Silica Fouling on Nonwetting Surfaces

Journal:	*Soft Matter*
Manuscript ID	SM-ART-02-2022-000165.R1
Article Type:	Paper
Date Submitted by the Author:	23-Mar-2022
Complete List of Authors:	Hatte, Sandeep; Virginia Polytechnic Institute and State University, Mechanical Engineering Pitchumani, Ranga; Virginia Polytechnic Institute and State University,

Analysis of Silica Fouling on Nonwetting Surfaces

S. Hatte and R. Pitchumani*

Advanced Materials and Technologies Laboratory

Department of Mechanical Engineering

Virginia Tech, Blacksburg, Virginia 24061-0238

ABSTRACT

Ground water sources used as coolant fluids in a variety of thermal systems such as heat exchangers and power plant condensers contain silica particles that accrete on heat transfer surfaces over time leading to reduction in thermal performance, a problem that is particularly exacerbated with temperature. Nonwetting superhydrophobic, lubricant-infused, and a new class of solid-infused surfaces introduced in this work are candidates for fouling mitigation, by virtue of their water repellency, but little is known about fouling of silica on the surfaces, especially under dynamic flow conditions and as a function of temperature. This article presents, for the first time, a systematic study of dynamic flow fouling of silica on nonwetting surfaces vis-à-vis conventional copper surface over a temperature range 20 °C – 50 °C. The mechanism of silica aggregate formation and its adherence to the different surfaces is elucidated by scanning electron microscope (SEM) imaging. Sigmoidal growth model is used to describe the time evolution of fouling thermal resistance and an Arrhenius model is presented for the temperature-dependent increase in the asymptotic fouling resistance on nonwetting and conventional surfaces alike. Lubricant-infused and solid-infused surfaces are shown to reduce fouling resistance by up to 25% and 13%, respectively, compared to conventional surface, whereas superhydrophobic surfaces lose their non-wettability under flow conditions, leading to an adverse increase in the fouling resistance by up to 13%. Considering the possible lubricant depletion in lubricant-infused surfaces over prolonged exposure to a flowing fluid, solid-infused surfaces present a robust alternative.

Keywords: silica fouling; superhydrophobic surface; lubricant-infused surface; solid-infused surface; Arrhenius relationship.

* Author for correspondence: pitchu@vt.edu

1. INTRODUCTION

Several energy transport systems utilize the flow of untreated water which contains undissolved salts/minerals in minute concentrations. Continuous contact of such solute particles with a heat transfer surface results in their gradual deposition. With time the deposits grow in size and spread throughout the surface. The lower thermal conductivity of such mineral foulants decreases the heat transfer performance of the system, therefore necessitating ways to mitigate the phenomenon of scale formation.[1-4] Among the different minerals, fouling by silica is of utmost importance owing to its presence in most ground water sources utilized in various applications.[5] As a result, understanding the mechanism of silica scale formation, quantification of reduction in heat transfer performance, and devising ways to mitigate fouling are necessary.

Several studies have been reported on the fouling of conventional heat transfer surfaces by silica.[5-10] Heuvel et al.[6] studied the effects of surface roughness on the early stages of silica scale formation. They observed that the precipitation of silica is strongly governed by the surface roughness; however, once silica has nucleated, further growth of and spread of aggregates is independent of surface morphology. Chan et al.[7] systematically studied the effects of supersaturation and Reynolds number on the scale formation of silica. Several other studies focused on the chemistry of silica aggregate formation, surface-silica interaction and quantification of the extent of fouling on smooth surfaces.[8-10]

Surfaces modified to induce nonwettability are viable options to deter fouling due to their propensity to repel water and thereby mitigate mineral accumulation. Nonwetting surfaces conventionally studied in the literature include superhydrophobic surfaces and lubricant-infused in which an air cushion or a lubricant fluid in the asperity interstices increases the water contact angle ($\gtrsim 120°$ and as high as 170°) and reduces the water sliding angle ($\lesssim 10°$ and as low as 2-3°).[11-12] Nonwetting surfaces have shown great potential for drag reduction[13-16], enhanced convection[17-18], enhanced phase change heat transfer[19], and reduced corrosion[20-21]. Use of nonwetting surfaces to deter fouling is also reported in the literature, focusing mostly on biofouling[22-24] whereas the limited studies on mineral fouling are restricted to calcium sulfate and calcium carbonate deposition on surfaces immersed in a *static fluid* medium.[25-27] In contrast, there is a little reported information on *dynamic flow fouling* on nonwetting surfaces. In our

previous study[28], we addressed this void by systematically investigating dynamic flow fouling of calcium sulfate and calcium carbonate on superhydrophobic and lubricant-infused surfaces, in comparison to smooth surfaces, and presented optimal surface designs for minimizing fouling resistance. The study highlighted the different nature of the fouling deposits and, in turn, the different fouling thermal resistance of the two minerals.

While calcium sulfate and calcium carbonate are the most considered minerals in fouling studies on nonwetting surfaces, since each mineral exhibits different deposition characteristics and, in turn, differs in the influence on the thermal performance, it is of interest to understand the nature of silica fouling on nonwetting surfaces. However, there is conspicuous absence of any information on silica fouling on nonwetting surfaces. In the present study, we fill this gap by systematic experiments of silica fouling on nonwetting copper surfaces in comparison to the conventional smooth copper surfaces. The nonwetting surfaces include superhydrophobic and lubricant-infused surfaces that are usually considered in the literature. Superhydrophobic surfaces (SHS) quickly lose their Cassie state of wettability, that underlies the extremely high water-contact angle, when exposed to a flowing fluid[28], and lubricant-infused surfaces (LIS) suffer from depletion of lubricant over time due to the shear from the flowing fluid, both leading to deterioration of nonwetting characteristics. To address these drawbacks, the study also introduces for the first time, a third class of nonwetting surface called *solid-infused surface* (SIS)[29], where the asperity valleys are infused with a polymer that is cured in place such that the surface of the polymer has a non-wetting characteristic. The solid infusion is expected to be robust to shear, thereby preserving the nonwetting properties of the surface over the long term.

First, using SEM imaging, the mechanism of silica aggregate formation and their adhesion and interaction with the four types of surfaces—SHS, LIS, SIS and smooth—is elucidated. Next, the extent of fouling on smooth and nonwetting surfaces is quantified in terms of fouling thermal resistance, for a range of foulant fluid flow temperature. The functional dependence of asymptotic fouling resistance on the flow temperature is expressed using Arrhenius relationship, which can be used to predict the temperature-dependent fouling performance of each surface for a range of temperature values. Overall, the study presents for the first time,

detailed information on temperature-dependent flow fouling of silica on conventional and nonwetting surfaces for practical relevance.

2. EXPERIMENTAL MATERIALS AND METHODS

2.1 Materials

Plain (smooth) Copper tubes of inner diameter 7.9 mm and outer diameter 8.7 mm are purchased from McMaster-Carr (Elmhurst, Illinois, USA) along with several cleaning agents namely methanol, ethanol and acetone. Chemicals utilized for the fabrication of rough superhydrophobic surfaces namely, hydrochloric acid, n-hexadecyl mercaptan are purchased from Fisher Scientific (Hampton, New Hampshire, USA). For lubricant-infused surface, Krytox 104 oil and for solid-infused surface a two-part Gentoo polymer are obtained from Miller-Stephenson (Danbury, Connecticut, USA). A colloidal silica solution is purchased from Sigma-Aldrich (St. Louis, Missouri, USA).

2.2 Surface Fabrication

Superhydrophobic surfaces were fabricated using the methods of chemical etching to generate roughness features inside a smooth copper tube followed by its functionalization. For etching, the samples were cleaned and covered on the outside and were immersed in a 1:1 by volume ratio of 12M hydrochloric acid and 3% hydrogen peroxide for 20 mins. The method of chemical etching, owing to the process of static immersion of samples in a solution bath, is scalable to different sample shapes and sizes. The cleaning procedure of all the samples was same where the samples were thoroughly washed with acetone. methanol and deionized (DI) water and air-dried before further procedure. Post etching, samples were washed thoroughly in DI water and dried at room temperature. Etched samples were then immersed in a bath of dilute solution of 0.02 mol$\cdot L^{-1}$ Mercaptan in ethanol at 50 ℃ for one hour. At this stage the samples were washed in ethanol and allowed to dry at room temperature.

For the fabrication of Krytox 104 infused LIS, chemically etched superhydrophobic surfaces were placed tilted and Krytox oil was dripped uniformly on the top half of the sample from one end and compressed air was used to spread the oil within the tube. The same procedure was

repeated from the other end until a uniform spreading of oil was achieved. After that, the oil was allowed settle down on the sample overnight before use.

For fabrication of SIS, the two parts of the Gentoo polymer solution were first mixed in a 1:1 ratio by weight and stirred for 120 minutes at room temperature. Next, the tube section was covered on the outer side and dipped into the Gentoo solution. Shortly after the dipping, the tube was rotated at around 1700 rpm for about 5 mins to uniformly spread the Gentoo solution within the surface and to avoid overfilling of the asperities. As a final step, the sample was cured at an elevated temperature of 90 $°C$ for one hour. Note that Gentoo polymer was used here to introduce the novel class of surfaces, based on its hydrophobic nature, ease of fabrication, thermal robustness, and durability. The fabrication process, however, applies to other polymers as well.

2.3 Experimental Setup and Procedures

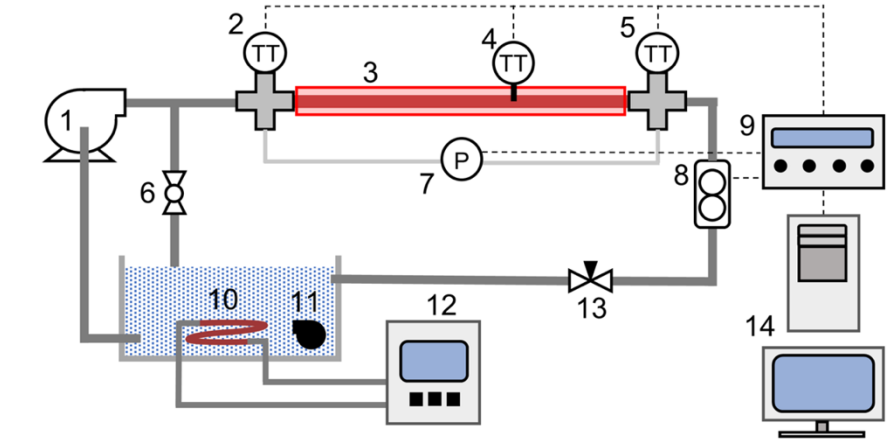

Figure 1: *Schematic of the setup for heat transfer fouling experiments.*

Figure 1 shows a schematic of the experimental setup used to quantify the extent of heat transfer fouling on various surface. The setup includes a tank with an agitation pump and chiller loop (10, 11), a centrifugal pump (1), a test section bypass line controlled by a ball valve (6), and the test section line controlled by a needle valve (13). The test section was heated by a set of heater jackets (3) that cover the entire sample length of 20 cm. A total of three RTDs (2, 4, 5) with accuracy of ±0.05°C are used for measuring test section inlet temperature (T_i), outlet temperature (T_o), and outer wall temperature (T_w), along with a magnetic flowmeter (8) with

accuracy of ±0.5% for measuring volumetric flowrate ($\dot{V}$) through the test section. The data acquisition was done using National Instruments temperature (NI-9216) and multifunction (NI-9381) input modules (9) and LabView 2020 (14).

During each experimental run, the tank was first filled with 10 L of water and both the pumps were switched on with the bypass line valve full open. The needle valve was then adjusted to achieve a desired volumetric flow rate, $\dot{V}$, based on a target Reynolds number (Re) for the experiment and the chiller recirculatory was switched on. Using the chiller recirculator the desired tank temperature was achieved. Next, the heater jacket was activated and set to desired heat flux (~3 kW/m^2) while overall system operation was monitored for steady state. At this stage, the data acquisition was started and allowed to run for 15 minutes to obtain steady state value of $\dot{V}$, T_i, T_o, and T_w. Next, the silica solution was added to the 10 L fluid tank to obtain an effective concentration of 1000 ppm. For the next several hours, the temperature and flow measurements are monitored. Once the outer surface temperature was observed to be saturated, the experiment was considered complete and the sample was removed and allowed to dry for 24 hours before SEM imaging.

2.4 Data Reduction

The heat transfer rate from the heater jackets to silica fluid flow is expressed as:

$$\dot{q} = \rho \dot{V} c_p (T_o - T_i) \tag{1}$$

where ρ, $\dot{V}$, c_p, T_i, and T_o are the density, flow rate, specific heat capacity, inlet temperature and outlet temperature of the silica solution, respectively. From this, the total heat transfer thermal resistance can be obtained as:

$$R_T = \frac{A_s}{\dot{q}} \cdot \frac{T_o - T_i}{ln\left(\frac{T_w - T_o}{T_w - T_i}\right)} \tag{2}$$

where A_s is the outer surface area of the tube. As the silica aggregates deposit on the inside of the tube, the total thermal resistance gradually increases. From the total resistance, the initial unfouled resistance R_T^0 corresponding to the case of flow of water without the presence of silica for first 15 mins is subtracted to obtain the fouling resistance as:

$$R_f = R_T - R_T^0 \tag{3}$$

3. RESULTS AND DISCUSSION

The process of chemical etching of smooth copper tubes results in the generation of roughness features. Figures 2a and 2b show the profilometric scans of a smooth and rough copper tube surface. It is evident from Figure 2a that smooth surface exhibits a more uniform profile with no discernible peaks and valleys, whereas Figure 2b shows the existence of asperities at several length scales. The surface profile in Figure 2b exhibits a maximum peak-to-valley height of ~12 μm, an average roughness value of ~6 μm and a root mean square (RMS) value of ~7.3 μm. For a smooth surface profile (Figure 2a), on the other hand, the maximum peak-to-valley height is measured to be ~0.70 μm, the average roughness is ~0.50 μm and the RMS value is ~0.55 μm. In addition, the multiscale features on etched copper tubes are quantified in terms of their fractal dimension (D), determined from a Fast Fourier Transform (FFT) based power spectrum of the surface profile[15,18,30] shown in Figure 2b, as $D = 1.70$. In comparison, for a smooth surface, the homogenous profile results in fractal dimension values closer to 1, $D \approx 1.05$ (Figure 2a). The information on the rough surface profiles, as presented in Figure 2b for a sample rough copper tube, was used in determining the amount of lubricant and solid infusion for fabrication of just-filled LIS and SIS.

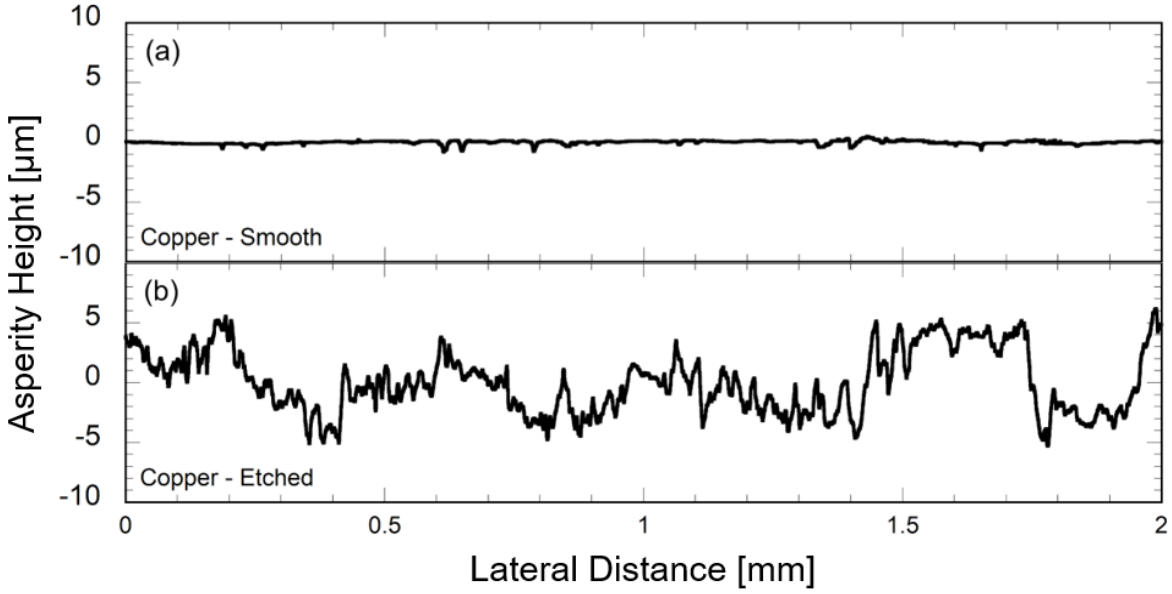

Figure 2: *Profilometric scans of (a) smooth and (b) etched copper tubes.*

Figure 3 shows the scanning electron microscope (SEM) images of smooth, superhydrophobic, lubricant-infused and solid-infused copper surfaces to reveal their structural information. Figure 3a shows that a smooth surface has no roughness features but a uniform appearance, also supported by the profilometric scan in Figure 2a. On such a smooth copper surface, the contact angle of water drop is less than 90° (70° in Figure 3a) categorizing it as a hydrophilic or wetting surface. On the other hand, all nonwetting surfaces—superhydrophobic, lubricant-infused and solid-infused surfaces—show apparent contact angle values greater than 90°, classifying them as hydrophobic surfaces. Figure 3b (along with the profilometric scan in Figure 2b) reveals the presence of asperities at multiple length scales on a superhydrophobic surface. Superhydrophobic surface (Figure 3b), by virtue of trapped air in the valleys offers extreme repellency to the water with contact angle of 161°, well in the superhydrophobic range of contact angle ≳150°.

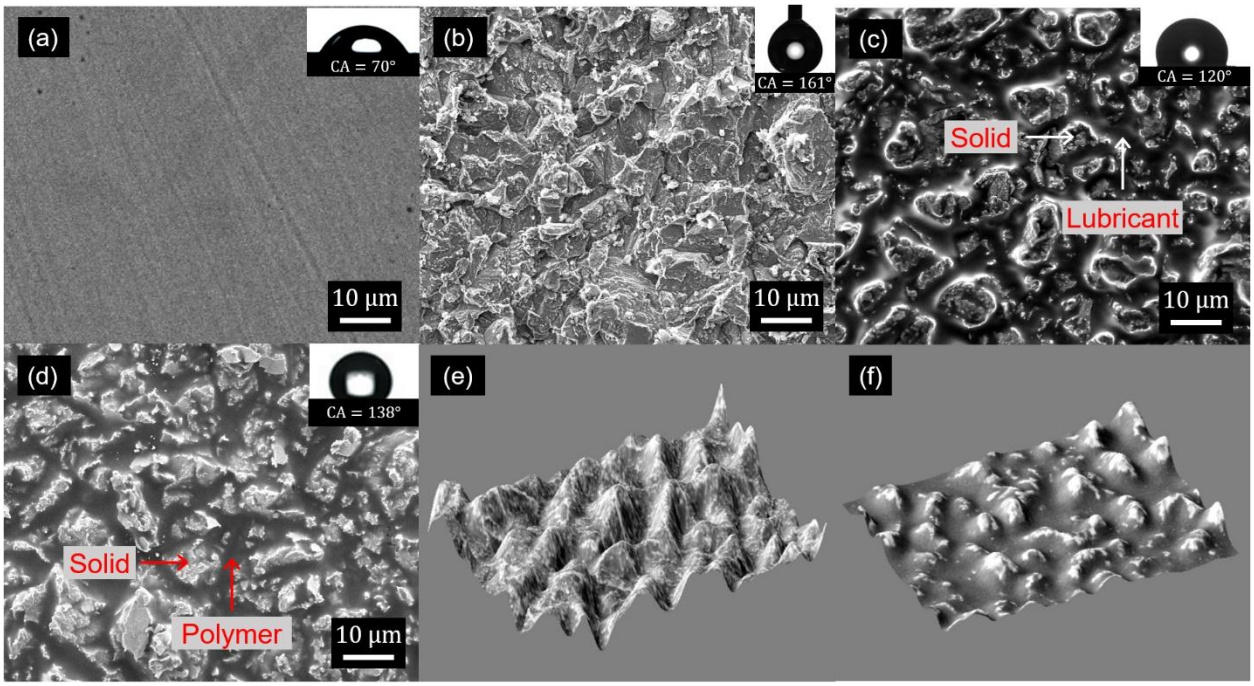

Figure 3: *SEM images of as-fabricated (a) smooth (b) superhydrophobic (c) lubricant-infused and (d) solid-infused surfaces, and three-dimensional isometric view of (e) as-fabricated etched surface and (f) Gentoo cured solid-infused surface.*

Figure 3c shows a lubricant-infused surface where the valleys of roughness features are impregnated with Krytox 104, where the brighter islands distributed within the black

background are the peaks of the asperities protruding out the infused lubricant, as marked. Owing to the slippery nature of the infused lubricant, LISs exhibit contact angle values in the range of 100–130°, as exemplified by the surface with a contact angle of 120° in Figure 3c. Figure 3d shows a solid-infused surface with cured Gentoo polymer (marked on the SEM) impregnated within the asperity valleys. Gentoo offers hydrophobic properties resulting in contact angle values in the range $110° - 150°$ (138° in Figure 3d). Figure 3d shows brighter regions of peaks protruding out of the cured Gentoo that fill the valleys at roughly the same level of the peaks of the asperities. The infusion of Gentoo can be distinctly seen by comparing the three-dimensional isometric views of an etched rough surface in Figure 3e with the Gentoo cured SIS in Figure 3f. Figure 3e shows the surface texture characterized by unfilled asperity valleys in an etched surface. The Gentoo polymer infused in the same surface shows the absence of deeper valleys indicating that the level of infused polymer is nearly at the same level as the top of the asperity elements.

Fouling characteristics of aforementioned four types of surfaces on the inside of copper tubes were studied using a forced convection heat transfer setup, shown in Figure 1, as per the experimental procedure described in section 2.3-2.4 to quantify the extent of fouling in terms of a fouling thermal resistance. Following each experiment, the samples are allowed to dry, and sections of each sample are observed under an SEM. Figure 4 shows a set of SEM images of silica fouled tubes with smooth, superhydrophobic, lubricant-infused and solid-infused inner walls.

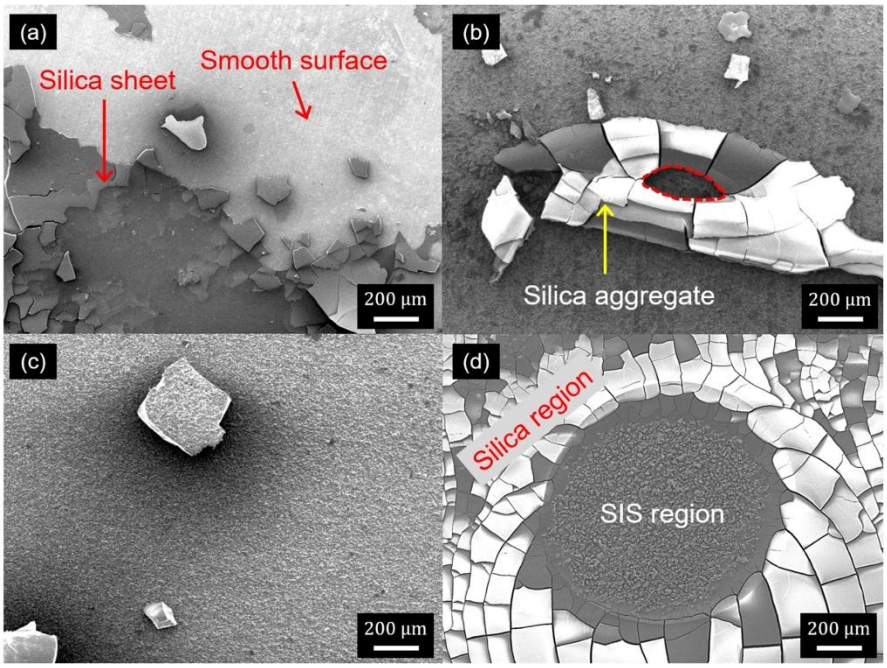

Figure 4: *SEM images of fouled (a) smooth (b) superhydrophobic (c) lubricant-infused and (d) solid-infused tube surfaces.*

Figure 4 collectively shows that silica deposition on surfaces is in the form of aggregates formed from the agglomeration of dispersed silica particles. Figure 4a exhibits that the silica aggregates have formed multiple layers of thin sheets covering the base smooth copper surface. Upon drying, the residual silica aggregates undergo crack formation as seen from Figure 4a. Figure 4b shows a region of silica-fouled superhydrophobic tube surface where a single larger aggregate of silica is seen. The central vacant part inside the aggregate as marked by red boundary is the region of residual dried droplet containing dispersed silica at the end of experimental run. The peripheral region undergoes solid aggregation of silica particles and undergoes crack formation upon drying. Similarly, Figure 4c shows a sparse distributed deposition of silica aggregates on a Krytox 104-infused LIS surface. For the case of Gentoo-infused SIS tubes, a similar pattern of deposition as in smooth surfaces is seen from Figure 4d. Figure 4d reveals silica aggregates in the form of sheets in one region and a distinct region left out by the evaporated residual drops at the end of an experimental run, as identified approximately by the circular region at the center.

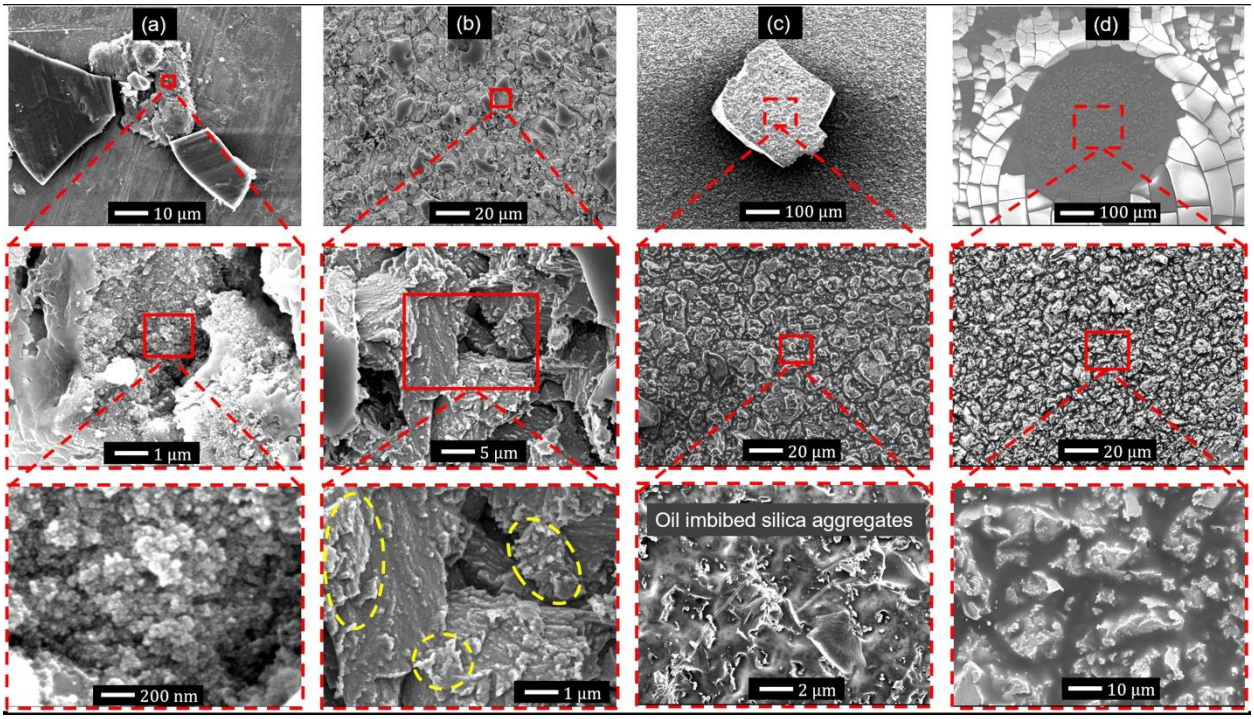

Figure 5: *Series of progressively zoomed-in SEM images of silica fouled (a) smooth (b) superhydrophobic (c) lubricant infused and (d) solid infused tube surfaces.*

Figure 5 shows the interaction between the different surface types used in the present study and silica aggregates. Figure 5a shows that for a smooth surface, a thin layer of silica aggregates stick to the surface and further growth of aggregates into larger bocks and sheets happens at random locations. From the zoomed-in images in the column of images under Figure 5a, it is evident that the silica aggregates are porous in nature with the smallest aggregate size resolved in the SEM imaging being around 50 nm. Dispersed silica particles have an average diameter of around 25 nm resulting in a closed packing of aggregates that are easily adhered to heat transfer surfaces. The interaction of SHS with the silica aggregates is strikingly different compared to smooth surface. The presence of peaks and valleys of lengths scales on the order of micrometers on an SHS results in the deposition of silica aggregates deep within the valleys and its further growth on the surface. Figure 5b shows a series of SEM images at increasing magnification that indicate the roots of larger silica aggregates are present either deep within the valleys or on the sides of the peaks, as identified by yellow regions in Figure 5b, resulting in higher strength of the overall aggregate structures. This observation further suggests that the air cushion in an as-

fabricated SHS that is the basis of the high Cassie state of nonwettability has been displaced by the flowing fluid, resulting a fully or partially Wenzel state of wettability.

LIS surfaces present an interesting interaction wherein the larger aggregates of silica imbibing the lubricant within their porous network. Figure 5c shows that larger silica aggregates have compact packing of silica agglomerates with the presence of oil that is binding the aggregates together. The presence of lubricant oil is also evident from the absence of cracks in the dried silica aggregates as compared to the other surface types. For the case of silica fouling on SIS surfaces, the pattern of deposition is divided into two categories, first is the region of deposition where the silica aggregates are formed into sheets on the surface, and the second is the region where the residual drops are dried and vacant circular holes are formed on the aggregates. The zoomed-in images of the central hole under Figure 5d show the bare SIS surface similar to Figure 3d, with no residue of silica aggregates.

Building on the qualitative information on the interaction of surface structure type and silica aggregates presented so far, Figure 6 quantifies the extent of fouling of silica onto the different heat transfer surfaces in terms of the variation of fouling resistance with time. Figure 6 shows that for all four surface types and for all average inlet temperature values of foulant flow, the fouling resistance first remains zero (Region 1) and then gradually increases with time (Region 2) followed by its asymptotic convergence to the asymptotic fouling resistance, $R_{f\infty}$ (Region 3). The three regions are illustrated in Figure 6a, but apply to all the surfaces. At $t = 0$ the induction of foulant in the flowing fluid does not result in its deposition onto heat transfer surface at the very beginning. With increasing time, the dispersed silica particles form deposits at several nucleation sites on the surface. At this stage, the force of adhesion by the surface attracts more foulant deposition and with its subsequent growth and spread on the heat transfer surface. During this period the fouling resistance increases with time. As the foulant deposits grow in size, the shear caused by the flowing fluid results in gradual removal of the deposited foulant. During this period the growth rate of thermal fouling resistance decreases. The competing effects of surface adhesion and shear by the flowing fluid results in an asymptotic fouling thermal resistance, as indicated in Figure 6a.

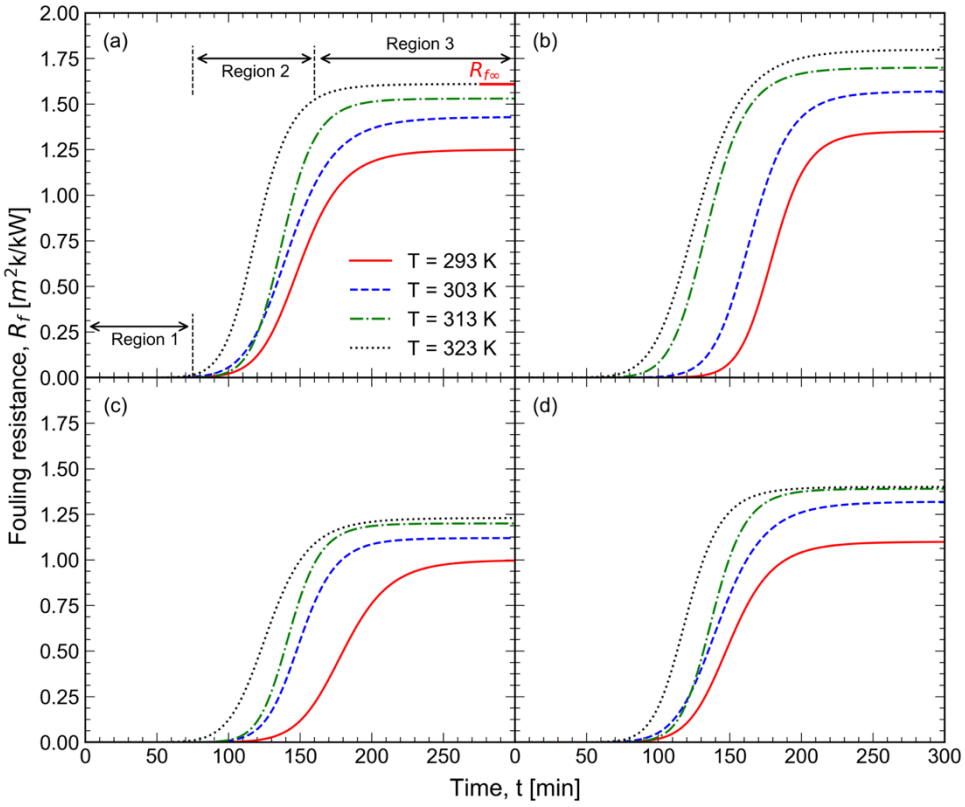

Figure 6: *Variation of fouling resistance, R_f, with time, t, for a range of fluid flow temperatures for (a) smooth, (b) superhydrophobic, (c) lubricant-infused and (d) solid-infused tube surfaces.*

The nature of fouling resistance variation with respect to time, seen in Figure 6, can be modeled by a sigmoidal growth curve expressed mathematically as:

$$R_f(t) = R_{f\infty}\left(1 - \frac{1}{1 + (t/t_0)^k}\right) \quad \#(4)$$

where $R_{f\infty}$ is the asymptotic fouling resistance, t_0 is the time instance of change of curvature of R_f vs t and k is a constant that relates to the rate of increase of fouling resistance at $t = t_0$. Figure 6 shows that for all four surface types, at any given time instant, a higher fluid flow temperature results in a higher fouling resistance. Increase in fouling resistance at any given time is attributed to two reasons: first, increase in fluid flow temperature increases the surface temperature thereby decreasing the surface tension of water, resulting in easy spreading and higher adhesion of foulant fluid on heat transfer surface. Over the range of temperature studied 20 °C to 50 °C, the interfacial water-air tension decreases from 72 mN/m to 67 mN/m.[31] In addition, at higher temperatures the kinetics of aggregation of silica particles significantly

increases[32] leading to the early deposition of larger aggregates and a greater rate of deposition, leading to higher fouling thermal resistance.

Figure 7 presents the variation of asymptotic fouling resistance, $R_{f\infty}$, with flow inlet temperature, T. It is evident from Figure 7a that for all temperature values considered in the study, the asymptotic fouling resistance increases with temperature, by about 33% for SHS and about 23%, 27% and 29% for the LIS, SIS and smooth surface, respectively. SHS consistently shows higher asymptotic thermal resistance followed by smooth surface, then Gentoo infused SIS surface and the least asymptotic thermal resistance is shown by Krytox 104 infused LIS. The higher asymptotic fouling resistance for SHS compared to smooth surfaces is attributed to the possible transition of flow from Cassie to Wenzel state. In the Wenzel state the foulant fluid flow penetrates the valleys of the rough asperities, resulting higher exposed area and exposure to more surface nucleation sites. Furthermore, the growth of silica aggregates within the valleys of SHS leads to the higher adhesion of deposit layers on to the SHS heat transfer surface.

In LIS, the presence of lubricant lowers the nucleation areas on the surface and further, since the flowing liquid glides easily on the surface, the interaction between the fluid and the surface is reduced, as seen from the least values of $R_{f\infty}$ in Figure 7a. The case of Gentoo infused SIS is unique, where the presence of cured polymer within the valleys of a rough surface results in an effective area for the deposition of foulant similar to that of a smooth surface. On the other hand, the hydrophobic nature of Gentoo reduces the interaction with the external fluid flow, leading to lower asymptotic fouling resistance compared to smooth surface. However, since the effective area for nucleation is greater for SIS than LIS, $R_{f\infty}$ for SIS is greater than that for LIS, as seen from Figure 7a. Overall, LIS and SIS show about 25% and 13% reduction in the asymptotic fouling resistance, respectively, compared to smooth surface, whereas SHS has a 13% *increase* in the asymptotic fouling resistance with respect to a smooth surface, over the entire range of temperature studied.

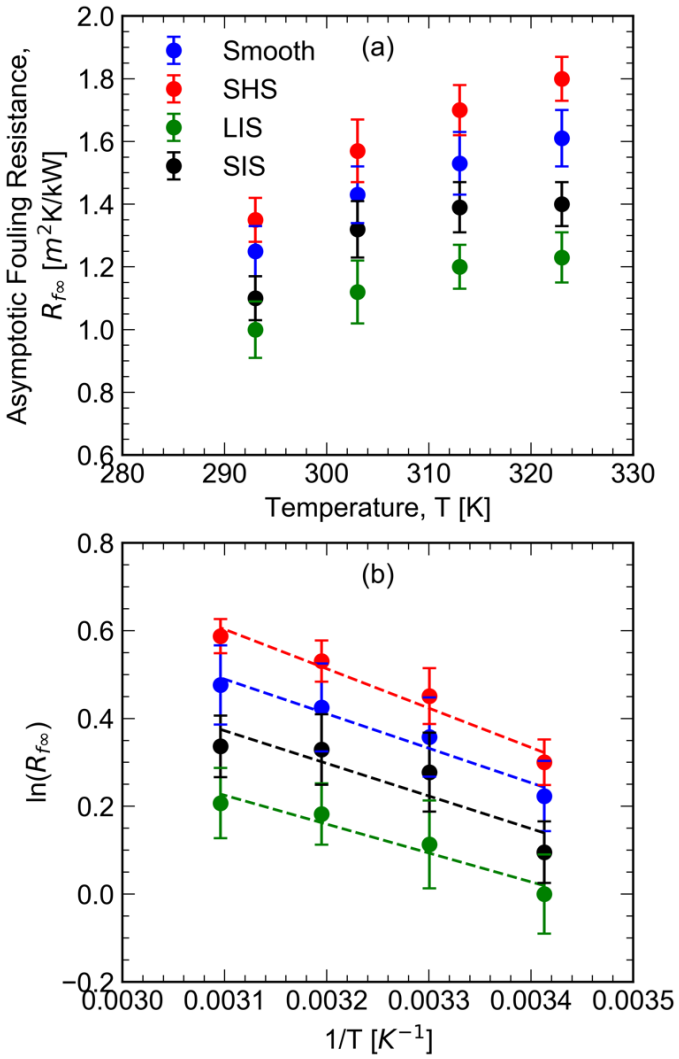

Figure 7: *Variation of asymptotic fouling resistance with flow temperature for all the surface types studied, and (b) Arrhenius relationship of $R_{f\infty}$ with absolute temperature.*

In order to establish a functional dependence of asymptotic fouling resistance with temperature, an Arrhenius relationship is used owing to the similarity of fouling kinetics to chemical reaction rates. The mathematical expression for the Arrhenius relationship is given as:

$$R_{f\infty} = R^*_{f\infty} e^{-\frac{T^*}{T}} \#(5)$$

where the pre-exponential factor $R^*_{f\infty}$ is the saturated asymptotic fouling resistance as, theoretically, the temperature, T, approaches infinity. As $T \to \infty$, the asymptotic fouling resistance theoretically saturates as the effects of increasing temperatures on the formation of larger aggregates and increasing adhesion of flowing fluid to the surface diminishes. The

exponential factor T^* determines an activation temperature value where the saturating asymptotic fouling resistance starts to build.

In the present study, the values of constants $R^*_{f\infty}$ and T^* for the four different types of surfaces were determined through a least-squares regression fit through the measured data of $R_{f\infty}$ with absolute temperature (in Kelvin). Figure 7b presents the measured $R_{f\infty}$ with the inverse of the absolute temperature on a semi-log plot, such the Arrhenius equation is a linear variation on this plot with a negative slope whose magnitude equates to $R^*_{f\infty}$, and the intercept of the line on the ordinate is $\ln T^*$. Figure 7b shows that the data points all lie closely along such straight lines, which confirms the Arrhenius nature of the temperature dependence of the asymptotic fouling resistance for all the four surfaces. The dashed lines in the plot denote the least-squares linear regression fits, from which the derived values of $R^*_{f\infty}$ and T^* are summarized in Table 1. It is evident from the values of $R^*_{f\infty}$ in Table 1, that LIS has the least saturation fouling resistance that is about one-half of the saturation resistance for a smooth surface and SIS presents about 23% lower saturation resistance compared to the smooth surface. In comparison, SHS has a 58% higher saturation fouling resistance relative to the smooth surface.

***Table 1**: Constants in Arrhenius relationship (eq. 5) for various surface types*

Surface type	$R^*_{f\infty}$	T^* [K]
Smooth	18.7	787
SHS	29.5	897
LIS	9.6	658
SIS	14.5	743

Solid-infused nonwetting surfaces were introduced for the first time in this article and their performance was assessed by considering silica fouling mitigation. The potential uses of the surfaces are many including boiling heat transfer enhancement, promoting dropwise condensation, corrosion mitigation, among others, which will be considered in future studies. The present study considered chemical etching as a common facile texturing method for comparison of SHS, LIS and SIS. The effects of other surface texturing methods (such as electrodeposition) to produce different asperity structures may be considered in a future study.

Similarly, the role of different infusion materials for LIS (for example, Krytox 101-105, silicone oils, etc.) and SIS (e.g. Sylgard), and a possible composite infusion of oils and polymers may also be pursued, building on the approach and results presented in this article. Durability of nonwetting surfaces is an important consideration, which is explored in separate studies[12,33], that the reader is referred to.

CONCLUSIONS

In the present study, systematic experiments are presented to elucidate, for the first time, the fouling kinetics of silica on smooth, superhydrophobic, lubricant-infused and solid-infused copper tube surfaces. Silica adhesion characteristics on the various surface types is demonstrated with scanning electron microscopic imaging. The extent of fouling is quantified in terms of a fouling thermal resistance and the following salient points were elucidated:

- SHS show consistently *higher fouling* by about 13% compared to smooth surface, owing to the Cassie to Wenzel transition that causes the silica dispersed fluid flow to penetrate and grow silica aggregates within the asperity valleys of SHS.
- Krytox 104 infused LIS exhibits the least fouling, about 25% *lower* than a smooth surface, owing to the presence of slippery infusion liquid within the valleys that offers reduced interaction between the surface and the fluid flow.
- Gentoo cured SIS demonstrated an appreciable fouling *reduction* of 13% compared to smooth surface, but higher fouling than LIS.
- Studies at the higher temperatures showed that the fouling increases with temperature for all surfaces, that can be described well using Arrhenius kinetics. Again, LIS and SIS demonstrated a lower increase of 23% and 27% in the asymptotic fouling resistance with temperature, compared to 29% for a smooth surface and a 33% increase for SHS.
- Overall, LIS presents a viable option for heat transfer surfaces to mitigate fouling by silica. However, considering the possible depletion of the beneficial lubricant in LIS over prolonged exposure to a flowing fluid, SIS presents a robust alternative.

ACKNOWLEDGEMENT AND DISCLAIMER

The material reported in this publication is based upon work supported by the U.S. Department of Energy under Award Number DE-FE0031556. This publication was prepared as an account of work sponsored by an agency of the United States Government. Neither the United States Government nor any agency thereof, nor any of their employees, makes any warranty, express or implied, or assumes any legal liability or responsibility for the accuracy, completeness, or usefulness of any information, apparatus, product, or process disclosed, or represents that its use would not infringe on privately owned rights. Reference herein to any specific commercial product, process, or service by trade name, trademark, manufacturer, or otherwise does not necessarily constitute or imply its endorsement, recommendation, or favoring by the United States Government or any agency thereof. The views and opinions of authors expressed herein do not necessarily state or reflect those of the United States Government or any agency thereof.

REFERENCES

[1] E. Nebot, J. F. Casanueva, T. Casanueva and D. Sales, Model for Fouling Deposition on Power Plant Steam Condensers Cooled with Seawater: Effect of Water Velocity and Tube Material. Int. J. Heat Mass Transf. (2007), 50 (17–18), 3351–3358. doi:10.1016/j.ijheatmasstransfer.2007.01.022.

[2] X. Zhao and D. C. Xiao, A Critical Review of Basic Crystallography to Salt Crystallization Fouling in Heat Exchangers. Heat Transfer Engineering 34.8-9 (2013): 719-732. doi:10.1080/01457632.2012.739482

[3] J. W. Suitor, W. J. Marner and R. B. Ritter, The History and Status of Research in Fouling of Heat Exchangers in Cooling Water Service. The Canadian Journal of Chemical Engineering 55.4 (1977): 374-380. doi:10.1002/cjce.5450550402

[4] H. Müller-Steinhagen, Heat transfer fouling: 50 Years After the Kern and Seaton Model. Heat Transfer Engineering 32.1 (2011): 1-13. doi:10.1080/01457632.2010.505127

[5] K. D. Demadis, Combating Heat Exchanger Fouling and Corrosion Phenomena in Process Waters. Compact Heat Exchangers and Enhancement Technology for the Process Industries, 483-490 (2003).

[6] D. B. van den Heuvel, E. Gunnlaugsson and L. G. Benning, Surface roughness affects early stages of silica scale formation more strongly than chemical and structural properties of the substrate. Geothermics, 87 (2020), 101835. doi.org/10.1016/j.geothermics.2020.101835

[7] S. H. Chan, H. Rau, C. DeBellis and K. F. Neusen, Silica fouling of heat transfer equipment—Experiments and model, (1988). doi.org/10.1115/1.3250583

[8] I. Gunnarsson and S. Arnórsson, Impact of silica scaling on the efficiency of heat extraction from high-temperature geothermal fluids. Geothermics, 34(3) (2005), 320-329. doi.org/10.1016/j.geothermics.2005.02.002

[9] C. Ning, L. Mingyan and Z. Weidong, Fouling and corrosion properties of SiO2 coatings on copper in geothermal water. Industrial & engineering chemistry research, 51(17) (2012), 6001-6017. doi.org/10.1021/ie202091b

[10] P. J. R. Schreier and P. J. Fryer, Heat exchanger fouling: a model study of the scaleup of laboratory data. Chemical engineering science, 50(8) (1995), 1311-1321. doi.org/10.1016/0009-2509(95)98843-4

[11] R. Jain and R. Pitchumani, Facile Fabrication of Durable Copper-Based Superhydrophobic Surfaces via Electrodeposition. Langmuir, 34(10) (2017), 3159-3169. doi.org/10.1021/acs.langmuir.7b02227

[12] R. Stoddard, K. Nithyanandam and R. Pitchumani, Fabrication and Durability Characterization of Superhydrophobic and Lubricant-Infused Surfaces. Journal of Colloid and Interface Science, 608, (2022), 662-672. doi.org/10.1016/j.jcis.2021.09.099

[13] S. Hatte and R. Pitchumani, Analytical Model for Drag Reduction on Liquid-infused Structured Non-wetting Surfaces. Soft Matter 17(5) (2021): 1388-1403. doi:10.1039/D0SM01272F

[14] Y. Tuo, H. Zhang, W. Rong, S. Jiang, W. Chen and X. Liu, Drag Reduction of Anisotropic Superhydrophobic Surfaces Prepared by Laser Etching, (2019). doi:10.1021/acs.langmuir.9b01040.

[15] S. Hatte and R. Pitchumani, Fractal Model for Drag Reduction on Multiscale Nonwetting Rough Surfaces. Langmuir 36, no. 47 (2020): 14386–14402. doi: 10.1021/acs.langmuir.0c02790.

[16] K. Kant and R. Pitchumani, Laminar Drag Reduction in Microchannels with Liquid infused Textured Surfaces. Chemical Engineering Science 230 (2021): 116196. doi:10.1016/j.ces.2020.116196

[17] S. Hatte and R. Pitchumani, Analysis of Laminar Convective Heat Transfer Over Structured Non-Wetting Surfaces, Int. J. Heat Mass Transf. 167 (2021) 120810. doi:10.1016/j.ijheatmasstransfer.2020.120810.

[18] S. Hatte and R. Pitchumani, Analysis of Convection Heat Transfer on Multiscale Rough Superhydrophobic and Liquid Infused Surfaces. Chemical Engineering Journal 424 (2021): 130256. doi:10.1016/j.cej.2021.130256

[19] R. Stoddard, K. Nithyanandam and R. Pitchumani, Steam Condensation Heat Transfer on Lubricant-infused Surfaces, IScience. 24 (2021) 102336. doi:10.1016/j.isci.2021.102336.

[20] S. M. A. Mousavi and R. Pitchumani, Bioinspired Nonwetting Surfaces for Corrosion Inhibition Over a Range of Temperature and Corrosivity. Journal of Colloid and Interface Science, 607, (2022), 323-333. doi:10.1016/j.jcis.2021.08.064

[21] S. M. A. Mousavi and R. Pitchumani, A Study of Corrosion on Electrodeposited Superhydrophobic Copper Surfaces. Corrosion Science, 186, (2021) 109420. doi:10.1016/j.corsci.2021.109420

[22] P. Zhang, L. Lin, D. Zang, X. Guo and M Liu, Designing Bioinspired Anti-Biofouling Surfaces based on a Superwettability Strategy. Small, 13(4) (2017) 1503334. doi:10.1002/smll.201503334

[23] M. Ferrari, and A. Benedetti, Superhydrophobic Surfaces for Applications in Seawater. Advances in colloid and interface science, 222 (2015) 291-304. doi:10.1016/j.cis.2015.01.005

[24] J. Genzer, and K. Efimenko, Recent Developments in Superhydrophobic Surfaces and Their Relevance to Marine Fouling: a Review. Biofouling, 22 (5) (2006) 339-360. doi:10.1080/08927010600980223

[25] S. B. Subramanyam, G. Azimi and K. K. Varanasi, Designing Lubricant-Impregnated Textured Surfaces to Resist Scale Formation. Advanced Materials Interfaces, 1 (2) (2014) 1300068. doi:10.1002/admi.201300068

[26] W. Jiang, J. He, F. Xiao, S. Yuan, H. Lu and B. Liang, Preparation and Antiscaling Application of Superhydrophobic Anodized CuO Nanowire Surfaces. Industrial & Engineering Chemistry Research, 54(27) (2015) 6874-6883. doi:10.1021/acs.iecr.5b00444

[27] M. F. B. Sousa, G. F. Barbosa, F. Signorelli and C. A. Bertran, Anti-scaling Properties of a SLIPS Material Prepared by Silicon Oil Infusion in Porous Polyaniline Obtained by Electropolymerization. Surface and Coatings Technology, 325 (2017) 58-64. doi:10.1016/j.surfcoat.2017.06.038

[28] S. Hatte and R. Pitchumani, Generalized Analysis of Dynamic Flow Fouling on Heat Transfer Surfaces. International Journal of Heat and Mass Transfer, (2022) 122573. doi:10.1016/j.ijheatmasstransfer.2022.122573.

[29] R. Pitchumani and R. Stoddard, Solid Infused Surfaces for High Efficiency Condensation, Provisional U.S. Patent 63/185,973.

[30] R. Jain and R. Pitchumani, Fractal Model for Wettability of Rough Surfaces. Langmuir, 33(28), (2017), 7181-7190. doi:10.1021/acs.langmuir.7b01524

[31] Engineering ToolBox, (2004). Surface Tension of Water in contact with Air.

[32] M. Tourbin and C. Frances, Monitoring of the Aggregation Process of Dense Colloidal Silica Suspensions in a Stirred Tank by Acoustic Spectroscopy. Powder technology, 190(1-2) (2009), 25-30. doi:10.1016/j.powtec.2008.04.067

[33] S.M.A. Mousavi and R. Pitchumani, A Comparative Study of Mechanical and Chemical Durability of Non-wetting Superhydrophobic and Lubricant-Infused Surfaces. Colloids and Surfaces A: Physicochemical and Engineering Aspects, 643, (2022) 128711. doi:10.1016/j.colsurfa.2022.128711.

FIGURE CAPTIONS

Figure 1. Schematic of the setup for heat transfer fouling experiments.

Figure 2. Profilometric scans of (a) smooth and (b) etched copper tubes.

Figure 3. SEM images of as-fabricated (a) smooth (b) superhydrophobic (c) lubricant-infused and (d) solid-infused surfaces.

Figure 4. SEM images of fouled (a) smooth (b) superhydrophobic (c) lubricant-infused and (d) solid-infused tube surfaces.

Figure 5. Series of progressively zoomed-in SEM images of silica fouled (a) smooth (b) superhydrophobic (c) lubricant infused and (d) solid infused tube surfaces.

Figure 6. Variation of fouling resistance, R_f, with time, t, for a range of fluid flow temperatures for (a) smooth, (b) superhydrophobic, (c) lubricant-infused and (d) solid-infused tube surfaces.

Figure 7. Variation of asymptotic fouling resistance with flow temperature for all the surface types studied, and (b) Arrhenius relationship of $R_{f\infty}$ with absolute temperature.